http://eprints.gla.ac.uk/184473/

Development of a broadband superluminescent diode based on self-assembled InAs quantum dots and demonstration of high-axial-resolution optical coherence tomography imaging

Nobuhiko Ozaki[1,*], Sho Yamauchi[1], Yuma Hayashi[1], Eiichiro Watanabe[2], Hirotaka Ohsato[2], Naoki Ikeda[2], Yoshimasa Sugimoto[2], Kenji Furuki[3], Yoichi Oikawa[3], Kunio Miyaji[3], David T. D. Childs[4], and Richard A. Hogg[4]

[1] *Faculty of Systems Engineering, Wakayama University, Wakayama 640-8510, Japan*
[2] *National institute for materials science (NIMS), Tsukuba, Ibaraki 305-0047, Japan.*
[3] *Think-Lands, Co., Ltd., Yokohama, Kanagawa 230-0046, Japan.*
[4] *School of Engineering, University of Glasgow, Glasgow, G12 8LT, U.K.*
*E-mail: ozaki@wakayama-u.ac.jp

Abstract

We developed a near-infrared (NIR) superluminescent diode (SLD) based on self-assembled InAs quantum dots (QDs) and demonstrated high-axial-resolution optical coherence tomography (OCT) imaging using this QD-based SLD (QD-SLD). The QD-SLD utilized InAs QDs with controlled emission wavelengths as a NIR broadband light emitter, and a tilted waveguide with segmented electrodes was prepared for edge-emitting broadband electroluminescence (EL) spanning approximately 1–1.3 μm. The bandwidth of the EL spectrum was increased up to 144 nm at a temperature of 25°C controlled using a thermoelectric cooler. The inverse Fourier transform of the EL spectrum predicted a minimum resolution of 3.6 μm in air. The QD-SLD was subsequently introduced into a spectral-domain (SD)-OCT setup, and SD-OCT imaging was performed for industrial and biological test samples. The OCT images obtained using the QD-SLD showed an axial resolution of ~4 μm, which was almost the same as that predicted from the spectrum. This axial resolution is less than the typical size of a single biological cell (~5 μm), and the practical demonstration of high-axial-resolution OCT imaging shows the application of QD-SLDs as a compact OCT light source, which enables the development of a portable OCT system.

Keywords: Quantum dot, Molecular beam epitaxy, Superluminescent diode, Optical coherence tomography

1. Introduction

Optical coherence tomography (OCT) has been intensively developed and widely used in various medical and biological fields as a non-invasive profile imaging tool since the first report by Huang et al. [1]. OCT relies on low-coherence interferometry, and the axial resolution (Δz) of an image is influenced by the bandwidth ($\Delta \lambda$) and center wavelength (λ_0) of its light source, e.g., expressed as $0.44 \times \lambda_0^2/\Delta \lambda$ for a light with a Gaussian spectral shape [2]. As OCT is used for medical applications, λ_0 of the light source should be in the near-infrared (NIR) region owing to the long penetration depth of NIR light in a biological sample [3]. Thus, a NIR broadband light source should be developed for high-axial-resolution OCT. In addition, the spectral shape of the light source should preferably be dipless, e.g., Gaussian, because a dip in the spectrum causes side lobes of the main peak in the point-spread function (PSF) of the light source, which results in noise in an OCT image and a reduction in the axial resolution [4].

To satisfy these requirements for an OCT light source, a considerable amount of effort have focused on the development of broadband light sources. Among various broadband light sources, a semiconductor-based light source device—a superluminescent diode (SLD), which is an electrically-driven diode with a high-intensity and broadband spectrum, has been developed. A SLD exhibits amplified spontaneous emission with a lower coherence than that of a laser diode, has a higher output power than that of a light-emitting diode, and has the advantages of being compact, robust, and relatively cost-friendly. However, a SLD typically utilizes conventional light emitting materials such as double heterostructures or multiple quantum wells, and it is difficult to broaden its spectrum. Thus, a self-assembled InAs quantum dot (QD) ensemble has been recognized as an ideal light-emitting material. InAs QDs grown on GaAs [5] are induced by strain due to the lattice mismatch between an epitaxially grown InAs layer and a GaAs substrate, i.e., the Stranski–Krastanov growth mode [6]. The inherent size and In composition distributions of the self-assembled InAs QD ensemble cause a broadband emission spectrum because of the bandgap energy modulation due to the quantum

size effect. In addition, InAs/GaAs QDs usually emit in the NIR region, e.g., 1–1.3 μm. These properties meet the requirements for an ideal OCT light source. Furthermore, this material can easily be applied for a semiconductor-based SLD device, and the QD-based light source can realize a compact and high-axial-resolution OCT system.

Many research groups have developed a SLD including self-assembled InAs QDs (QD-SLD) [7–23]. However, few reports have assessed the development of QD-SLDs as an OCT light source; only a limited number of reports describe the theoretical axial resolution via its PSF [11, 18, 20–22], and even fewer show OCT imaging based on the light source [13]. In the present work, we developed and introduced a QD-SLD into an OCT system and demonstrated OCT imaging to evaluate its potential as a compact OCT light source. Although we previously reported OCT imaging of a cover glass plate, which is a flat and highly reflective sample [22], [24], OCT imaging of a biological sample was difficult because of high light scattering in biological samples. Thus, we developed a QD-SLD with a tilted waveguide and segmented contacts and utilized a thermoelectric cooler (TEC) to increase the output power and extend the bandwidth of the QD-SLD. With these improvements, we experimentally demonstrated the feasibility of the QD-SLDs for OCT imaging of biological samples. In particular, we focused on the criterion of the axial resolution, i.e., less than 5 μm, which is required for the resolution of single cells in a biological sample [25].

2. Experiment

2.1 QD-SLD chip fabrication

A QD-SLD was fabricated on an n^+-GaAs (001) substrate wafer using the molecular beam epitaxy (MBE) method. Figure 1(a) shows a schematic profile of the QD-SLD. A 240-nm-thick GaAs waveguide layer, which includes four stacked layers of self-assembled InAs-QDs (QD1–4), was sandwiched between p-/n-Al$_{0.35}$Ga$_{0.65}$As cladding layers for optical and electronic confinement. Each embedded QD layer was capped with a strain-reducing layer (SRL) [26],

3

which consisted of $In_{0.2}Ga_{0.8}As$, with different thicknesses (approximately 0, 1, 2, and 4 nm) to realize sequential shifts in the emission center wavelength of the QDs. As previously reported, the combination of shifted QD emission using the SRL was effective for broadening the spectrum and tailoring its spectral shape [19, 27, 28]. In particular, it can be applied to fill the spectral dip between the discrete emission peaks of each InAs QDs layer.

A ridge-type waveguide (RWG) was fabricated on the grown wafer using photolithography and dry-etching techniques. After deposition and area-selective wet-etching of the SiO_2 thin insulation film on the RWG, contact electrodes were formed on both sides of the wafer. Subsequently, the wafer was cleaved to form a 4-mm-long SLD chip. Figure 1(b) shows a plan-view schematic of the QD-SLD chip. A RWG with a 5-μm-width and 1.4-μm-height, which was tilted approximately 6° from normal to the cleaved edge, was prepared in this work, because the tilted RWG configuration reduces the back reflections of the propagating light at the cleaved edges and avoids the occurrence of lasing in a certain cavity mode. This can be effective for broadening the SLD emission spectrum. The tilted RWG was covered with segmented electrodes with approximately 40-μm-wide contact gaps for the p-side contact. The segmented electrodes divide the current injection region into four segments; thus, a higher current density than a single electrode for the same injection current can be applied. This process induces spectrum broadening because of the higher current-density-derived state-filling of the higher excited states in the QDs, and emission spanning was extended to a shorter wavelength [22]. Moreover, the remaining segments where no current was applied could function as an optical absorber of the emission from the QDs in the segment for the injection current. In addition to the tilted waveguide configuration, this segmented electrode avoids lasing in the chip and can contribute to further broadening of the QD-SLD emission spectrum.
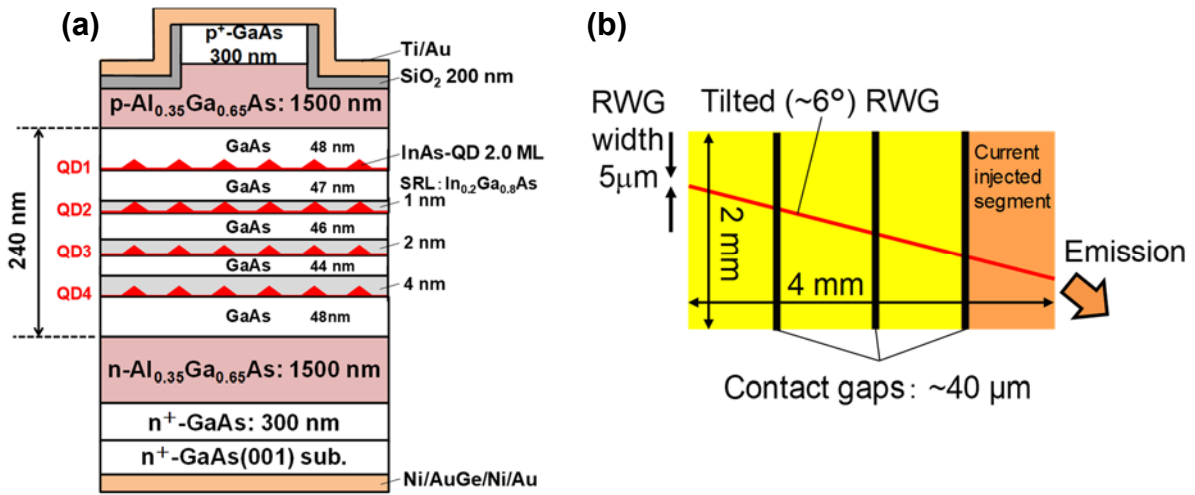
4

Fig. 1. (a) Schematic profile of a fabricated QD-SLD.
(b) Illustration of the RWG and segmented contact electrodes fabricated for the QD-SLD.

2.2. SMF-coupled light source including the QD-SLD chip

The fabricated QD-SLD chip was installed in a module coupled to a single-mode optical fiber (SMF) to deal with the edge-emitted light from the QD-SLD chip through the SMF, as shown in Fig. 2. A TEC was installed under the chip carrier to control the chip operation temperature. The operation temperature was set at 25 °C. The SMF-coupled QD-SLD module was introduced into an OCT setup, which is described hereinafter. We prepared the QD-SLD module and a typical commercial SLD for reference as OCT light sources. In general, a commercial SLD includes a bulk or quantum well semiconductor emitter, and its spectrum is narrower than that of the self-assembled QD-based SLD.
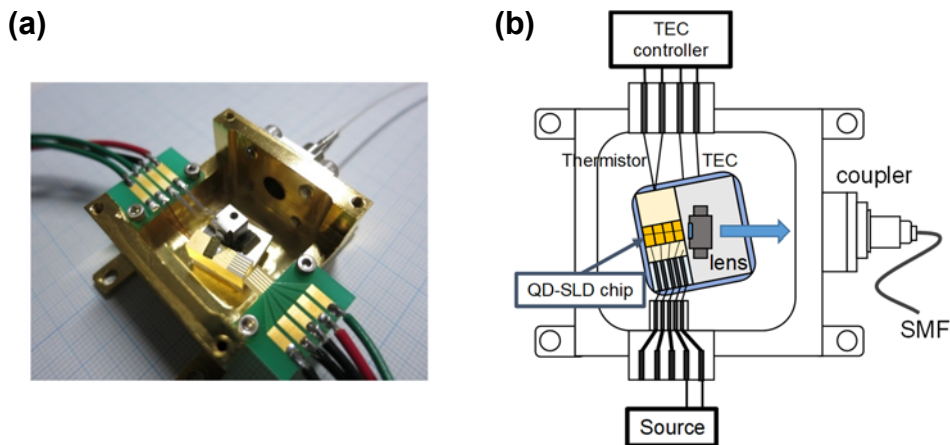

Fig. 2. (a) Photograph and (b) schematic of a SMF-coupled module including the fabricated QD-SLD chip.

5

Their emission spectra, detected by an optical spectrum analyzer (OSA) are presented in Figs. 3(a) and 3(c). The peak wavelengths and bandwidths were approximately 1340 and 60 nm, respectively, for the commercial SLD at an injection current of 300 mA and approximately 1100 and 144 nm, respectively, for the QD-SLD at an injection current of 250 mA. The spectrum of the QD-SLD is broader than that of the commercial SLD, indicating the effectiveness of the self-assembled InAs QDs for obtaining broadband emission compared with the conventional semiconductor material. This broadband emission is mainly due to the inherent size and In composition distributions of the InAs ensemble. In addition, the emission peak wavelengths of the stacked InAs QD layers were sequentially shifted using SRLs with different thicknesses [19], and a broadband and dipless spectrum was obtained. The peak wavelength of the spectrum of the commercial SLD was almost the same while the injection current increased, whereas that of the QD-SLD varied with the increasing injection current. The peak wavelength was blue-shifted from approximately 1230 nm to 1100 nm. This can be attributed to the state-filling effect, where supplied carriers filled the discrete states in the QDs in a stepwise manner from lower energy states to higher energy states with increasing injection current, as previously reported [21,22]. A blue-shift can occur at a relatively lower injection current owing to the lower number of states in a QD compared with a bulk semiconductor or quantum well, and it is beneficial for extending the span of the emission spectrum.

The output powers measured through the SMF were 1.4 mW for the commercial SLD and 2.3 μW for the QD-SLD. Considering that the QD-SLD chip has only four active layers of QDs and there exists a relatively large coupling loss between the as-cleaved edge of the chip and the non-coated SMF, the output power could be smaller than that of the commercial SLD. However, the absolute output power does not significantly influence the axial resolution of OCT imaging. This is because the OCT image is based on the interference signal between the reflections from the sample and reference mirror, and the interference signal intensity is critical for the axial resolution rather than the absolute power of the light source.

6

Figures 3(b) and 3(d) present the inverse Fourier transform (IFT) EL spectra shown in Figs. 3(a) and 3(c), respectively. According to the Wiener–Khinchin theorem [29], the IFT power spectrum of the light source corresponds to the autocorrelation function, and the full width at half maximum (FWHM) of the autocorrelation provides a theoretical estimate of the axial resolution (Δz) as the light source is used in an OCT system. The estimated values of Δz of each SLD are 13.6 and 3.6 µm. These values are more accurate estimates than that using the formula presented in Section 1, i.e., $0.44 \times \lambda_0^2/\Delta\lambda$, because this can only be adopted for a light source with a Gaussian spectral shape in the frequency domain.
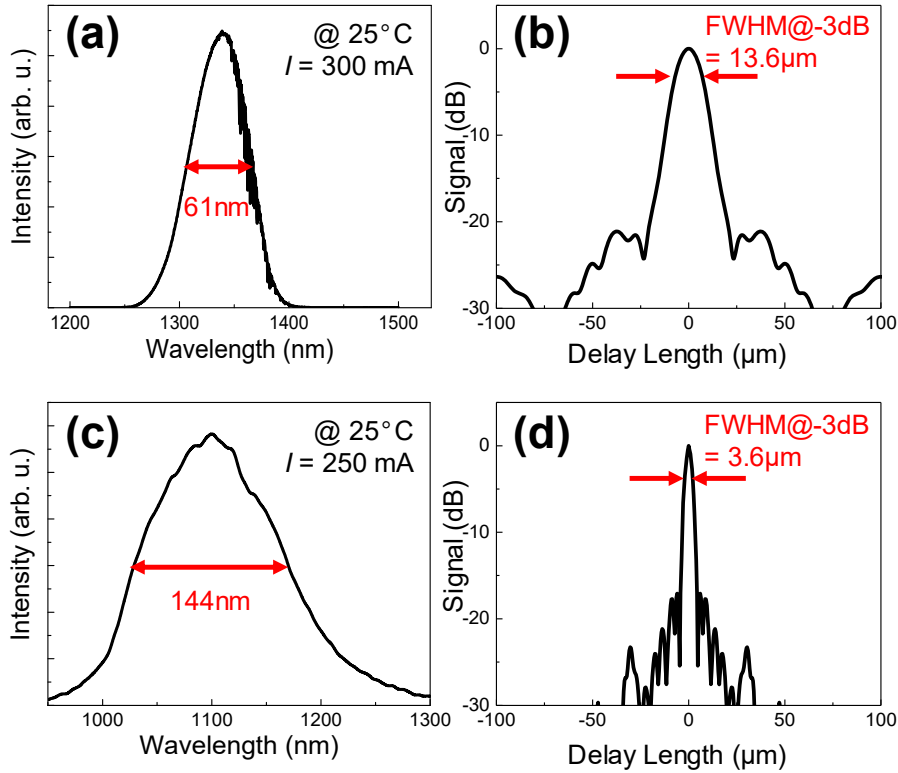

Fig. 3. EL spectra ((a) and (c)) and IFT spectra ((b) and (d))
obtained from a typical commercial SLD and QD-SLD, respectively.

2.3. Spectral-domain (SD) OCT setup

We employed a spectral-domain (SD)-OCT system to demonstrate OCT imaging. SD-OCT is a method of obtaining an OCT image using the IFT spectrum of an interference signal

between the reflections from the sample and reference mirror [30]. Figure 4 schematically shows that we constructed a SD-OCT interferometer consisting of a low-coherence light source, a reference arm, a sample arm, and an optical spectrometer. The low-coherence light from the introduced SLD modules propagated through a SMF was split by a 50:50 coupler, and directed into the reference and sample arms. The reflected light from both arms were recombined by the coupler, and the optical spectrometer measured the interference spectrum.

To sample the interference signals, we employed the OSA or an InGaAs multi-channel detector attached to a spectrometer. The InGaAs detector was cooled with liquid nitrogen, and spectra with a high signal-to-noise ratio can be obtained even from a sample with high light scattering and low reflection, including a biological sample. The IFT of sampled interference signal spectrum was performed using commercial software and a workstation. Before the IFT operation, the sampled signal was rescaled to k by linear interpolation, and the number of data points on both sides of the spectrum was added using the zero-filling method [24].
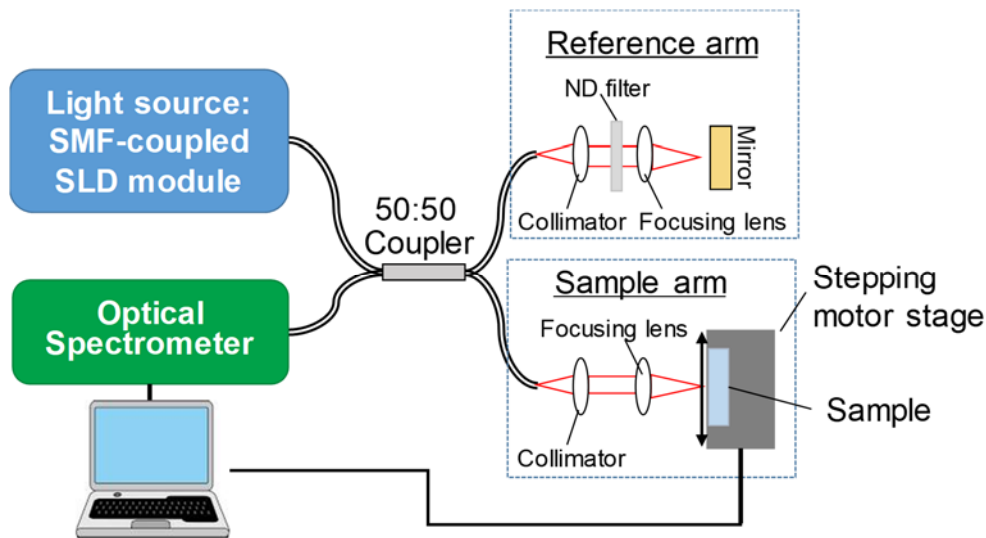

Fig. 4. Schematic of the SD-OCT setup with the introduced QD-SLDs.

We prepared a 5-µm-thick transparent film for SD-OCT imaging to evaluate the axial resolution of the SLDs. The 5-µm-thick transparent film was a nitrocellulose membrane whose refractive index was 1.4–1.5. This refractive index is similar to that of biological sample (~1.4) and the membrane has a flat surface at the boundaries with air; thus, this is available for testing

8

at an actual axial resolution less than 5 μm. In addition, we prepared plant samples: a slice of onion and a leaf of cabbage as a biological phantom. The samples were placed on a stepping-motor-driven stage and moved in the lateral direction to obtain a 2D OCT image. The light probe was focused on the sample using a lens, and the probe diameter was approximately 10 μm, which corresponds to the lateral resolution.

3. Results and Discussion

3.1 PSF and axial resolution evaluation

We first validated the PSF by considering the auto-correlation function of the SLDs. The auto-correlation function was obtained from the IFT interference spectrum between the reflections from the mirrors set in the reference and sample arms. Figure 5 summarizes the interference spectra and deduced PSF for the commercial SLD for reference and the QD-SLD. The FWHMs of the PSFs for the SLDs, which represent the actual axial resolutions (Δz) in air of SD-OCT, were estimated to be 14.2 and 4.2 μm, respectively. The values of Δz obtained from the PSF were slightly (0.6 μm) larger than theoretical values of Δz estimated from the IFT EL spectra shown in Figs. 3(b) and 3(d). This difference can be attributed to the influence of the dispersion of the optical components used in the SD-OCT setup, such as the focusing lenses. The light sources have broadband spectra; thus, the dispersion of the optical components affected the interference signal and resulted in a reduction in the axial resolution. However, the axial resolution of the QD-SLDs was less than that of the commercial SLD and can be expected to be less than 5 μm, which is a criterion for single-cell resolution.
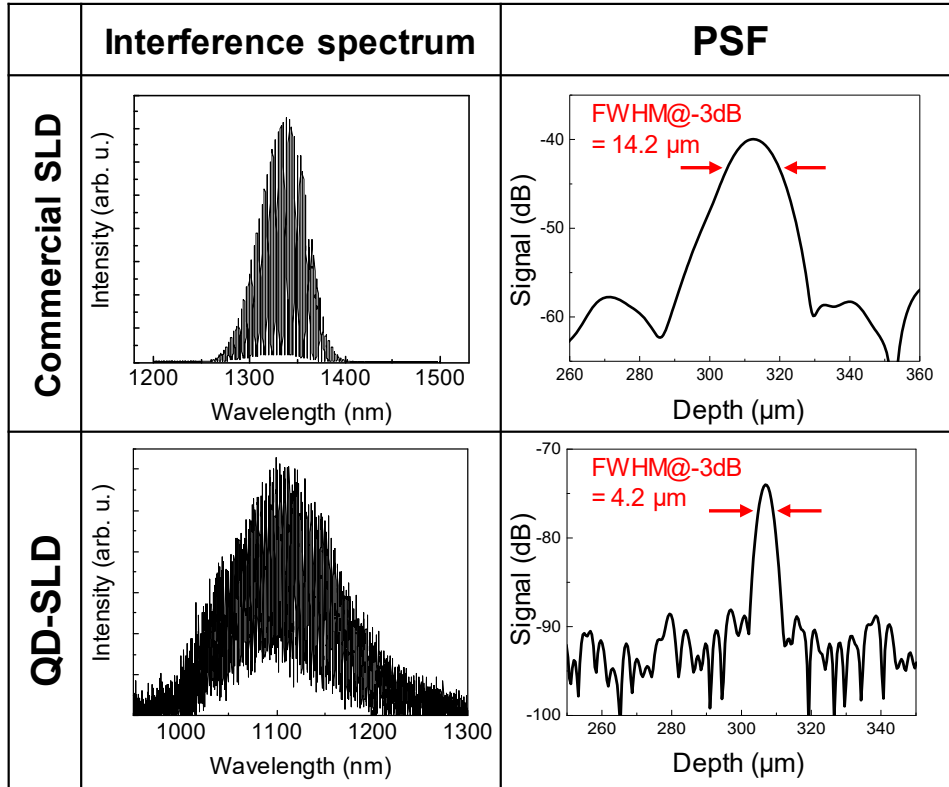
Fig. 5. Comparison of the interference spectrum and PSF for the commercial SLD and QD-SLD.

3.2. OCT imaging of a thin-film sample

We then performed OCT imaging for a test sample using the QD-SLD. First, a 5-μm-thick film sample was observed using the SD-OCT setup. Figure 6 presents the 2D OCT images obtained using the commercial SLD (upper) and QD-SLD (lower). The light probe vertically illuminated the film and laterally scanned it. Two white narrow lines were clearly shown in the OCT images obtained using the QD-SLD, whereas a broad line was seen in the OCT image obtained using the commercial SLD. The two white lines resulted from reflections at both surfaces of the film; thus, the distance between the two peaks represented the optical path length in the film. The depth profile at the origin of the lateral axis in the image showed that the distance was approximately 7.3 μm, which almost corresponded to the physical thickness of the film (5 μm) multiplied by its refractive index, i.e., 1.4–1.5. In contrast, in the depth profile of the commercial SLD, the peaks were not resolved; thus, the thickness of the film could not be determined because the FWHM of the PSF of the commercial SLD was 14.2 μm (in air) and

10

the convoluted spectra of the two boundaries were combined, forming a broad band spectrum.

From these results, a higher axial resolution less than 5 μm was demonstrated using the QD-SLD as an OCT light source.

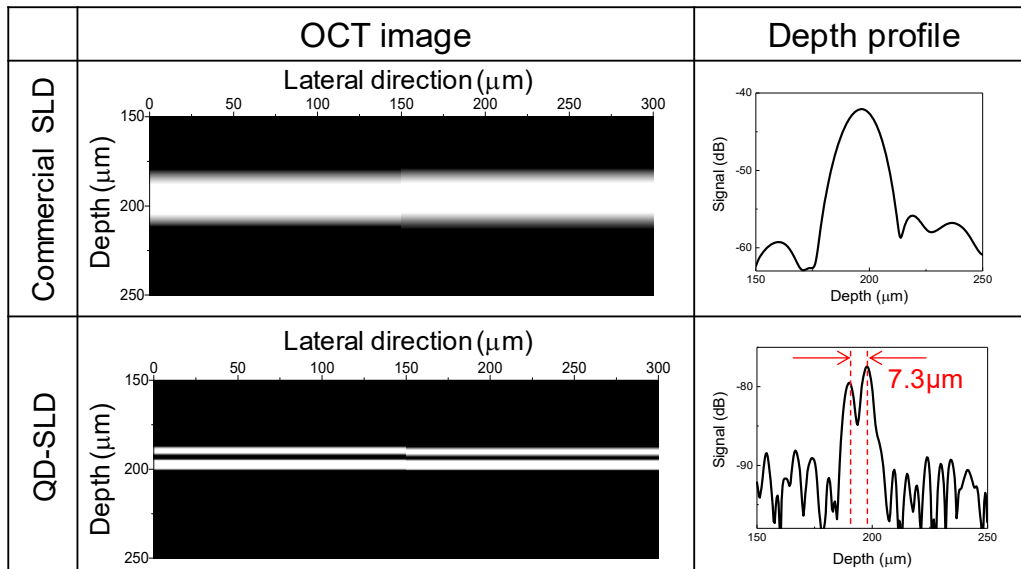Fig. 6. Comparison of the OCT images of a 5-μm-thick film using the commercial SLD and QD-SLD. Each depth profile is obtained at the origin in the lateral direction (left edge) of the OCT image.

3.3. OCT imaging of biological samples

Finally, we performed OCT imaging for biological samples. Figure 7 presents OCT images of an onion slice. The light incident axis was normal to the sample surface, which corresponds to the depth direction, and the sample was scanned in the lateral direction. The upper and lower images were obtained at the same position in the sample using the commercial SLD and QD-SLD, respectively. The comparison shows that the image resolution was improved by using the QD-SLD; the surface of the sample and the interfaces of cells appeared with narrower white lines. In the depth profiles obtained at 50 μm in the lateral direction, as indicated by a red dashed line in each image, several peaks indicating reflection from the cell boundaries were observed. The distance between the peaks was in the range of approximately 40–60 μm, which corresponds to the cell size of the onion. The FWHMs of each peak in the depth profile were

approximately 14 and 4 μm for the commercial SLD and QD-SLD, respectively. These values correspond to the FWHMs of their PSFs. These results demonstrated OCT imaging for a biological sample using the QD-SLD.
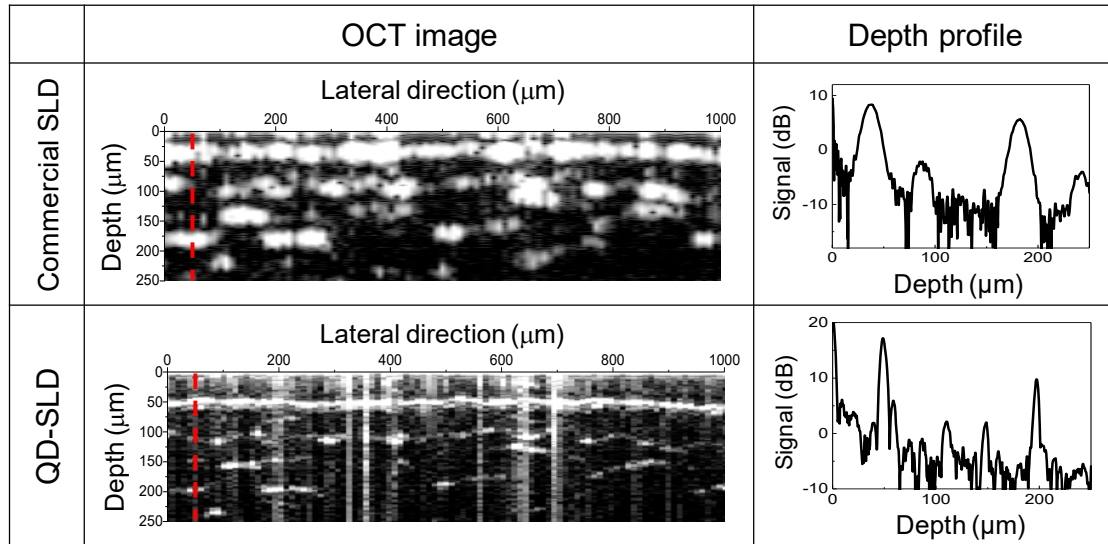

Fig. 7. Comparison of OCT images and depth profiles of an onion slice obtained using the commercial SLD and QD-SLD.

We then attempted to image the other biological sample, a leaf of cabbage, which contains smaller cells than those of the onion. Figure 8(a) shows an optical microscope plan-view image of a cabbage leaf observed by OCT. The incident light probe was normal to the leaf and scanned in the lateral direction across the vein, as indicated by the red line in Fig. 8(a). Figure 8(b) shows the OCT images obtained using the commercial SLD (upper) and QD-SLD (lower). A comparison of these images demonstrates the higher resolution obtained using the QD-SLD. A vein was seen at the middle of the OCT image as a black hole underneath a cell layer, as magnified in Fig 8(c). Generally, a plant leaf forms a layered structure, which consists of an upper epidermis, a palisade cell layer, and a spongy parenchyma cell layer. A vein exists between the palisade and spongy parenchyma cell layers. The palisade layer is a comparatively dense cell layer compared with the spongy cell layer, and light scattered in the palisade layer and at the boundary between the palisade and spongy parenchyma cell layers could be seen as apparent contrast in the OCT images. In addition, a vein that consisted of tiny tissues of xylem

and phloem filled with water and soluble organic compounds existed. Thus, low-intensity reflection was caused by the vein, and it appeared in the OCT image as a black hole. Fig. 8(d) shows the depth profiles at the center of each image shown in Fig. 8(c). The origin of the depth was set at the top surface (upper epidermis) of the sample in each image. Several reflection peaks appeared between the top surface and the lower boundary of the vein. It is noted that the fine peaks in the depth profile of the QD-SLD image can be distinguished, whereas they were combined into broad peaks in the profile of the image acquired by the commercial SLD. The smallest peak distance in the profile was approximately 3.5 μm, as indicated in the depth profile. This suggests that fine cells or scattering structures with sizes of approximately 4 μm in the palisade cell layer could be resolved by the QD-SLD.
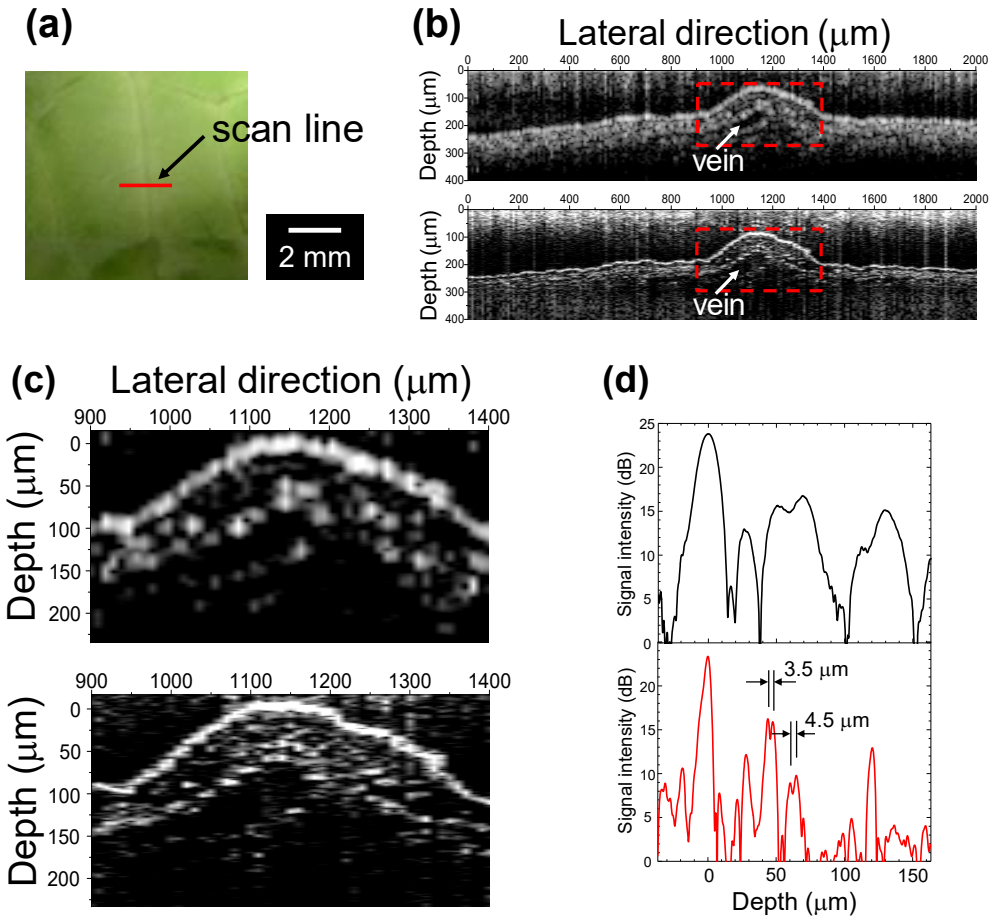

Fig. 8 (a) Plan-view optical microscope image of a cabbage leaf under OCT observation. The lateral scan line is indicated by a red line. (b) Comparison of the OCT images of the cabbage leaf acquired by the commercial SLD and the developed QD-SLD. (c) Magnified vein images from the red dashed-rectangular areas in Fig. 8(b). (d) Depth profiles at the center of the images shown in Fig. 8(c).

13

The abovementioned results demonstrate the high-axial-resolution and non-destructive observation of the inner tissues of plants using an OCT system with the QD-SLD light source. This investigation tool is useful in the study of plants and various *in-situ* studies for biological samples.

4. Conclusions

High-axial-resolution OCT imaging has been demonstrated using a NIR broadband light source based on self-assembled InAs QDs. The axial resolution achieved in the OCT images was less than 5 μm (~4 μm in air). The surfaces of a transparent film sample were distinguished, and its thickness was determined to be less than 5 μm using the QD-SLD with a spectrum whose FWHM and center wavelength were 144 and 1100 nm, respectively. Furthermore, we demonstrated OCT imaging of plant samples and realized an apparent improvement in the axial resolution of the image using the developed QD-SLD. From the abovementioned results, the QD-SLD-introduced OCT demonstrated potential as a useful biological sample observation tool. The QD-SLD is available as a compact OCT light source with high-axial-resolution, and this enables the development of a small and portable OCT system.

References

[1] D. Huang, E. A. Swanson, C. P. Lin, J. S. Schuman, W. G. Stinson, W. Chang, M. R. Hee, T. Flotte, K. Gregory, C. A. Puliafito, J. G. Fujimoto, Science **254**, 1178 (1991).

[2] M. E. Brezinski, *Optical coherence tomography: principles and applications* (Academic Press, 2006).

[3] M. S. Patterson, B. C. Wilson, D. R. Wyman, Lasers in Medical Science **6**, 379 (1991).

[4] C. Akcay, P. Parrein, J. P. Rolland, Appl. Opt. **41**, 5256 (2002).

[5] L. Goldstein, F. Glas, J. Y. Marzin, M. N. Charasse, G. Le Roux, Appl. Phys. Lett. **47**, 1099 (1985).

[6] I. N. Stranski and L. Von Krastanov, Akad. Wiss. Math.-Nat. Kl. IIb **146**, 797 (1938).

[7] Z. Z. Sun, D. Ding, Q. Gong, W. Zhou, B. Xu, Z. G. Wang, Optical Quant. Electron. **31**, 1235 (1999).

[8] Z. Y. Zhang, Z. G. Wang, B. Xu, P. Jin, Zh. Sun, and F. Q. Liu, IEEE Photonics Technol. Lett. **16**, 27 (2004).

[9] M. Rossetti, A. Markus, A. Fiore, L. Occhi, and C. Velez, IEEE Photon. Technol. Lett. **17**, 540 (2005).

[10] S. K. Ray, K. M. Groom, M. D. Beattie, H. Y. Liu, M. Hopkinson, and R. A. Hogg, IEEE Photonics Technol. Lett. **18**, 58 (2006).

[11] P. D. L. Greenwood, D. T. D. Childs, K. M. Groom, B. J. Stevens, M. Hopkinson, and R. A. Hogg, IEEE J. Sel. Top. Quantum Electron. **15**, 757 (2009).

[12] Z. Y. Zhang, R. A. Hogg, X. Q. Lv, and Z. G. Wang, Adv. Opt. Photonics **2**, 201 (2010).

[13] N. Krstajic, L. E. Smith, S. J. Matcher, D. T. D. Childs, M. Bonesi, P. D. L. Greenwood, M. Hugues, K. Kennedy, M. Hopkinson, K. M. Groom, S. MacNeil, R. A. Hogg, R. Smallwood, IEEE J. Sel. Top. Quantum Electron. **16**, 748 (2010).

[14] X. Li, P. Jin, Q. An, Z. Wang, X. Lv, H. Wei, J. Wu, J. Wu, Z. Wang, Nanoscale Res. Lett. **6**, 625 (2011).

[15] M. Tsuda, T. Inoue, T. Kita, and O. Wada, Phys. Status Solidi C **8**, 331 (2011).

[16] M. A. Majid, M. Hugues, S. Vézian, D. T. D. Childs, R. A. Hogg, IEEE Photonics J. **4**,

2066 (2012).

[17] S. Chen, M. Tang, Q. Jiang, J. Wu, V. G. Dorogan, M. Benamara, Y. I. Mazur, G. J. Salamo, P. Smowton, A. Seeds, and H. Liu, ACS Photonics **1**, 638 (2014).

[18] N. Ozaki, T. Yasuda, S. Ohkouchi, E. Watanabe, N. Ikeda, Y. Sugimoto, and R. Hogg, Jpn. J. Appl. Phys. **53**, 04EG10 (2014).

[19] N. Ozaki, K. Takeuchi, Y. Hino, Y. Nakatani, T. Yasuda, S. Ohkouchi, E. Watanabe, H. Ohsato, N. Ikeda, Y. Sugimoto, E. Clarke, and R. A. Hogg, Nanomat. Nanotechnol. **4**, 26 (2014).

[20] S. Chen, W. Li, Z. Zhang, D. Childs, K. Zhou, J. Orchard, K. Kennedy, M. Hugues, E. Clarke, I. Ross, O. Wada, R. Hogg, Nanoscale Res. Lett. **10**, 340 (2015).

[21] T. Yasuda, N. Ozaki, H. Shibata, S. Ohkouchi, N. Ikeda, H. Ohsato, E. Watanabe, Y. Sugimoto, and R. A. Hogg, IEICE Trans. Electron. **E99-C,** 381 (2016).

[22] N. Ozaki, D. T. D. Childs, J. Sarma, T. S. Roberts, T. Yasuda, H. Shibata, H. Ohsato, E. Watanabe, N. Ikeda, Y. Sugimoto, and R. A. Hogg, J. Appl. Phys. **119**, 083107 (2016).

[23] R. Yao, N. Weir, C. Lee, and W. Guo, IEEE Photonics J. **8**, 1601007 (2016).

[24] H. Shibata, N. Ozaki, T. Yasuda, S. Ohkouchi, N. Ikeda, H. Ohsato, E. Watanabe, Y. Sugimoto, K. Furuki, K. Miyaji, and R. A. Hogg, Jpn. J. Appl. Phys. **54**, 04DG07 (2015).

[25] J. Welzel, Skin Res. Technol. **7**, 1 (2001).

[26] K. Nishi, H. Saito, S. Sugou, and J.-S. Lee, Appl. Phys. Lett. **74**, 1111 (1999).

[27] N. Ozaki, K. Takeuchi, S. Ohkouchi, N. Ikeda, Y. Sugimoto, H. Oda, K. Asakawa, and R. A. Hogg, Appl. Phys. Lett. **103**, 051121 (2013).

[28] N. Ozaki, K. Takeuchi, S. Ohkouchi, N. Ikeda, Y. Sugimoto, K. Asakawa, R. A. Hogg, J. Cryst. Growth **323**, 191 (2011).

[29] L. Cohen, IEEE Signal Proc. Lett. **5**, 292 (1998).

[30] W. Drexler and J. G. Fujimoto, *Optical Coherence Tomography: Technology and Applications* (Springer 2008).